

# ADAPTING THE HYPERSPHERE LOSS FUNCTION FROM ANOMALY DETECTION TO ANOMALY SEGMENTATION

Joao P. C. Bertoldo, Santiago Velasco-Forero, Jesus Angulo, Etienne Decencière

MinesParis, PSL University, Centre for mathematical morphology (CMM), 77300 Fontainebleau, France  
 {jpcbertoldo, santiago.velasco, jesus.angulo, etienne.decenciere}@minesparis.psl.eu

## ABSTRACT

We propose an incremental improvement to Fully Convolutional Data Description (FCDD), an adaptation of the one-class classification approach from anomaly detection to image anomaly segmentation (a.k.a. anomaly localization). We analyze its original loss function and propose a substitute that better resembles its predecessor, the Hypersphere Classifier (HSC). Both are compared on the MVTec Anomaly Detection Dataset (MVTec-AD) – training images are flawless objects/textures and the goal is to segment unseen defects – showing that consistent improvement is achieved by better designing the pixel-wise supervision.

**Index Terms**— Anomaly Detection, Anomaly Segmentation, Loss Function, One-class Classification

## 1. INTRODUCTION

Anomaly Detection (AD) aims to identify deviations or non-membership to a class (a semantic concept of normality) by learning from normal instances and none or very few examples of such irregularities. In the past few years, this unsupervised problem has seen an increasing number of publications with novel approaches and several literature reviews [1, 2]. Computer Vision in particular has received considerable attention thanks to public datasets like the MVTec Anomaly Detection Dataset (MVTec-AD) [3], which contains industrial images of objects/textures and defines an AD problem both on the image level and on the pixel level. Image-wise AD consists of flagging which images contain a defect, while pixel-wise AD, a.k.a. *anomaly segmentation* (or localization), consists of marking which pixels belong to a defect (ground truth masks are available).

In this paper, we incrementally build on top of Fully Convolutional Data Description (FCDD) [4], a model that outputs, by design, a heatmap (see Figure 1) from the last feature map of a convolutional neural network by applying a Support Vector Data Description (SVDD)-inspired loss pixel-wise. We reformulate the Hypersphere Classifier (HSC) loss function to the segmentation task (initially designed for the image-wise setting), and Critical Difference (CD) diagrams using the Wilcoxon signed rank test (a non-parametric version of

the paired T-test) demonstrate consistent improvement in performance with less training epochs.

## 2. RELATED WORK

FCDD [4] is inspired by modifications of SVDD, a One-Class Classification (OCC) model. In this section we summarize the predecessors that led to its formulation, focusing on their incremental changes. For the sake of clarity, some details have been omitted, such as regularization terms. An extensive review of OCC models can be found in [5].

OCC was first formulated as an adaptation of *Support Vector Machines* (SVMs) that learns to separate anomalous data points from the origin with a hyperplane [6] or a hypersphere [7] in the feature space. The latter, *SVDD* [7], minimizes the radius of a hypersphere by incentivizing (via slack variables) the normal/anomalous data points to fall inside/outside the hypersphere. In other words, normal and anomalous instances are penalized in opposite directions, therefore (respectively) pulling towards and pushing away from the center – notice that this formulation assumes supervision.

One-Class Deep SVDD [8], a deep-learning model inspired by SVDD, applies a neural network  $\phi_\omega$  with parameters  $\omega$  to normal instances  $x_i \in \mathbb{R}^d$ , obtaining feature vectors  $\phi_\omega(x_i) \in \mathbb{R}^{d_F}$ , which are trained by minimizing

$$\frac{1}{n} \sum_{i=1}^n \|\phi_\omega(x_i) - a\|^2, \quad (1)$$

where  $a \in \mathbb{R}^{d_F}$  is the center of the hypersphere in the feature space and  $n$  is the number of instances in the batch. In other words, the mean squared Euclidean distance to the center  $a$  is minimized, and this distance is used as an anomaly score at inference time. Notice that this version does *not* consider anomalous instances, which makes the training less stable and (eventually) leads to feature collapse ( $\phi_\omega$  converging to a constant function).

Among several strategies proposed to prevent feature collapse, [9, 10] proposed an extension of (1) that brings in back the possibility of using supervision (therefore using normal and anomalous instances at training time) by applying

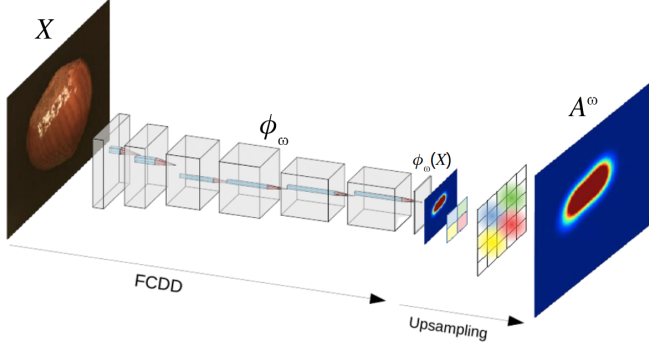


**Fig. 1.** Fully Convolutional Data Descriptor (FCDD). A pre-trained (and fine-tuned) convolutional neural network without fully connected layers is combined with an extra  $1 \times 1$  convolution layer to generate locality-preserving feature vectors. In the last (low resolution) layer, the distances to the hypersphere’s center are upsampled to the network’s input resolution and used as an anomaly score heatmap. Adapted from [4].

$$p(\cdot) = -\log(1 - \exp(-\cdot)), \quad (2)$$

to the anomalous instances’ scores, thus creating an incentive that *pushes* their (learned) feature vectors away from the center (we call  $p : \mathbb{R}^+ \rightarrow \mathbb{R}^+$  the “push” function). Besides the squared distance  $\|\cdot\|^2$  in Equation 1 was replaced by the Pseudo-Hubert function  $h(\cdot) = \sqrt{\|\cdot\|^2 + 1} - 1 \in \mathbb{R}^+$  as it is more robust to outliers, resulting in the Hypersphere Classifier (HSC) loss function:

$$\frac{1}{n} \sum_{i=1}^n (1 - y_i) h(\phi_\omega(x_i) - a) + y_i p(h(\phi_\omega(x_i) - a)), \quad (3)$$

where  $y_i$  is 0/1 if  $x_i$  is normal/anomalous respectively.

Finally, FCDD, illustrated in Figure 1, reused the HSC to directly segment anomalies by design. The first layers of a backbone convolutional neural network (e.g. VGG) feed a feature map to an extra (learnable)  $1 \times 1$  convolution added on top of it. At inference time, a low-resolution anomaly score map, or “heatmap”, is generated (from the pixel-wise vectors’ distances to the center of the hypersphere) and upsampled to the input resolution – a more formal formulation is presented in the next section.

Numerous other approaches (unlike the OCC) exist and will not be covered here, but a few major research branches are worth noting. Autoencoders (reconstruction models more generally) have been extensively studied and improved for anomaly detection tasks, and some variations still remain in the state-of-the-art (SOTA) [11]. Combinations of deep learning-based feature extraction with classic machine learning models like k-Nearest Neighbors [12, 13] and multivariate

Gaussian [14, 15] also achieve effective results despite their simplicity, and recent improved versions are also in the SOTA [16, 17]. However, nowadays most SOTA methods are based on pre-trained feature extractors combined with normalizing flows [18].

Our work aims to contribute towards closing the performance gap between OCC models and the current SOTA by finding a better loss function for [4], explained in Section 3, and our results, in Section 5, demonstrate its effectiveness.

### 3. LOSS FUNCTION

In this section we first present FCDD’s loss function (4), then propose our version (5), and finally describe its rationale by comparing them.

Let  $X \in \mathbb{R}^{n \times m}$  be a batch of  $n$  images of  $m$  pixels (spatial dimensions confounded) and  $Y \in \{0, 1\}^{n \times m}$  its respective batch of ground truth anomaly masks (0 means “normal”, 1 means “anomalous”), where  $X_{ij}$  refers to the pixel indexed by  $j \in \{1, \dots, m\}$  in the image  $X_i$ , indexed by  $i \in \{1, \dots, n\}$  ( $Y_{ij}$  defined accordingly).

First, the neural network  $\phi_\omega : \mathbb{R}^m \rightarrow \mathbb{R}^{d_F \times m'}$ , with parameters  $\omega$ , generates a feature map  $\phi_\omega(X_i) \in \mathbb{R}^{d_F \times m'}$  with low-resolution  $m'$  ( $m' < m$ ) and  $d_F$  features for each pixel. Then, a  $1 \times 1$  convolution with bias outputs a single value per pixel – the following notation considers this convolution (and its parameters) included in  $\phi$ , and the center  $a$  has been omitted as it is implicitly embedded in it. Finally, the Gaussian kernel-based upsampling operator outputs the anomaly score map  $A_i^\omega = \text{upsample}(h(\phi_\omega(X_i))) \in (\mathbb{R}^+)^m$  (indices defined as for  $X_{ij}$ ), where  $h(\cdot)$  is the Pseudo-Hubert function applied pixel-wise. [4] optimizes the parameters  $\omega$  by minimizing the loss function

$$\frac{1}{n} \sum_{i=1}^n \left[ \left( \frac{1}{m} \sum_{j=1}^m (1 - Y_{ij}) A_{ij}^\omega \right) + p \left( \frac{1}{m} \sum_{j=1}^m Y_{ij} A_{ij}^\omega \right) \right]. \quad (4)$$

We propose, as a substitute to Equation (4), the following loss function

$$\frac{1}{nm} \sum_{i=1}^n \sum_{j=1}^m (1 - Y_{ij}) A_{ij}^\omega + \frac{|J^0|}{|J^1|} Y_{ij} p(A_{ij}^\omega), \quad (5)$$

where  $J^y = \{(i, j) \in \{1, \dots, m\} \times \{1, \dots, n\} \mid Y_{ij} = y\}$  for  $y \in \{0, 1\}$  are, respectively, the sets of image and pixel indices of all normal and anomalous pixels in a batch.

Equation (4) is the cross-image average ( $\frac{1}{n} \sum_{i=1}^n$ ) of the sum of two terms that *look* like per-image averages ( $\frac{1}{m} \sum_{j=1}^m$ ) of anomaly scores on the normal pixels and on the anomalous pixels (left and right respectively). In fact,  $Y_{ij}$  zeroes part of the iterands, so the  $\frac{1}{m} \sum_{j=1}^m$  terms do not converge to any expected value. By correcting that, one would have  $p$  applied to



Fig. 2. Synthetic anomalies generated with confetti noise.

the *average score* of the anomalous pixels (not each pixel individually), which interferes with the backpropagation: (very) high-scored pixels can compensate the others blocking the propagation through (very) low-scored pixels. Therefore we propose to apply  $p$  on each pixel individually.

With these modifications, one would achieve a nested average (cross-image outside, cross-pixel inside). However, we propose to take the average directly on all the pixels in the batch ( $\frac{1}{nm} \sum_{i=1}^n \sum_{j=1}^m$ ) because otherwise the nested averages would give more weight to smaller anomalies. Finally, we scale the anomalous pixels’ scores by a factor  $\frac{|J^0|}{|J^1|}$ , compensating the imbalance of normal/anomalous pixels, which our tests have shown to be effective (details omitted for brevity) – other (more modern and effective) techniques to compensate imbalanced datasets exist but we deliberately do not focus on that subject.

#### 4. EXPERIMENTS

We aim to demonstrate that our proposed loss function improves from its baseline, therefore we test it with the same procedure as in [4] (a few differences specified below) on MVTEC-AD – 10 categories of object (e.g. “transistor”) and 5 categories of texture (e.g. “leather”), each category being trained and tested independently.

Procedure: a VGG-11, pre-trained on ImageNet, frozen up to the third max-pooling and cut before the fourth max-pooling is used; the network is fine-tuned using Stochastic Gradient Descent (SGD) with a batch size of 128 images, Nesterov momentum of 0.9, weight decay of  $10^{-4}$ , and initial learning rate of  $10^{-3}$  decreasing by a factor of 1.5% at each epoch.

One epoch is defined as 10 iterations over the training set with each image having 50% chance to be replaced by an anomalous image (before the data preprocessing/augmentation described below), which can be synthetic or real depending on the experiment (never both in the same training). Synthetic anomalies (unsupervised setting): automatically generated by superposing a confetti noise – randomly sized, placed, and colored squares – over the normal image, and the modified pixels are considered anomalous (Figure 2). Real anomalies (semi-supervised): one (randomly chosen) image of each anomaly type (between 1 and 6 types according to the

MVTec-AD category) is transferred from the test set to the training set. Notice that our focus is on the unsupervised setting but the semi-supervised setting (“a few” anomalies available) is also tested for reference.

Each experiment was repeated six times with different seeds, and the performance is measured in terms of run-wise average of two metrics: pixel-wise Area Under the Receiver Operator Characteristic curve (AUROC) and pixel-wise Average Precision (AP). Differences with [4]: we run the gradient descent for 50 epochs instead of 200, and the synthetic anomalies are not smoothed on the borders.

The training images are pre-processed and augmented in the following sequence: resize to 240 x 240; with 50% chance each, resize to 224 x 224 or crop to 224 x 224 in a random position; apply color jitter with all parameters set to 0.04 or all parameters set to 0.0005 with 50% chance each; apply Gaussian noise with zero mean and standard deviation set to 10% of the image’s pixel values’ standard deviation (all channels confounded) with 50% chance on each pixel; apply local contrast normalization (all channels confounded); normalize the data between 0 and 1 (min-max normalization). The test images are resized to 224 x 224 then the last two last two steps from above are applied.

We ran our experiments on two cluster nodes PowerEdge C4130 (processor Xeon E5-2680 V4, 7 cores, 2.4GHz), each with four GPUs Tesla P100-SXM2 (16 GiB), and we used Weights & Biases to monitor our experiments. The minimum GPU memory requirement is 5.6 GiB, and the (category-specific) average run time spans from 33 minutes to 2 hours. We used the code publicly provided by [4] with modifications to integrate the losses described in Section 3.

#### 5. RESULTS

Tables 1 and 2 compare the cross-category average results obtained with the baseline loss from [4] (Equation 4) and ours (Equation 5) in terms of, respectively, AUROC and AP. The baseline results in terms of AUROC are both copied from [4] (with “\*”) and reproduced by us. Category-specific scores available on GitHub: [gist.github.com/jpcbertoldo/8db759487279a5eec6fd0fc36764a4b4](https://gist.github.com/jpcbertoldo/8db759487279a5eec6fd0fc36764a4b4).

Figure 3 shows CD diagrams (with each metric) using the pairwise Wilcoxon signed-rank test with Bonferroni-Holm correction with a (nominal) significance level of  $\alpha = 10\%$  (probability of a type I error) considering the two-sided alternative hypothesis.

The Wilcoxon signed-rank test’s null hypothesis is that two methods are expected to rank similarly (“they have the same performance”) for any dataset, and non-parametrically compares their cross-dataset performance differences – notice that the categories in MVTEC-AD can be considered as independent datasets because they are trained and tested individually. In other words, it provides a stronger statistical argument (than comparing average performances) because rejecting its

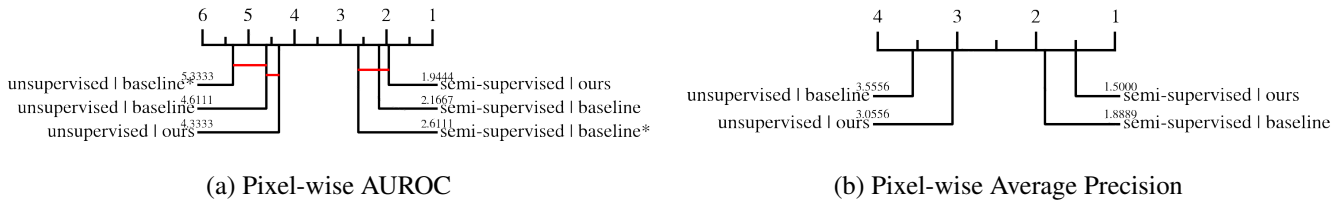


**Fig. 3.** Critical difference diagrams from the category-specific scores on the MVTec AD dataset using the Wilcoxon signed-rank test with the Bonferroni-Holm correction with a confidence level of  $\alpha = 10\%$  at for each pair of methods. Values on the scale are average rankings, and the methods within a same horizontal bar (a clique) are *not* significantly different according to the pair-wise statistical test. The scores of the methods marked with “\*” are from [4].

null hypothesis (i.e. methods that are not connected by a horizontal red bar in Figure 3) means that a method is (in general) significantly better than another regardless of the dataset (all other factors fixed).

**Table 1.** Pixel-wise Area Under the ROC curve (AUROC) scores (values in percentage) on the MVTec AD dataset. Cross-category average scores and cross-category average standard deviation (in parenthesis). Under the same supervision (group of three columns), the best performance is in bold. The columns “baseline\*” is from [4].

	semi-supervised		
	baseline*	baseline	ours
objects	95.2*	95.7 (1.4)	<b>95.8 (1.4)</b>
textures	97.0*	97.8 (0.4)	<b>97.9 (0.4)</b>
all	95.8*	96.4 (1.0)	<b>96.6 (1.0)</b>

	unsupervised		
	baseline*	baseline	ours
objects	91.0*	<b>92.5 (1.1)</b>	92.5 (1.0)
textures	92.8*	92.8 (1.3)	<b>94.1 (0.7)</b>
all	91.6*	92.6 (1.1)	<b>93.1 (0.9)</b>

## 6. DISCUSSION

As shown in Tables 1 and 2 the our modifications provided, on average, an increase in performance – categories “metal nut” and “tile” had the highest improvements (see the link to the full per-category table in Section 5). The average scores over object, texture, and all classes confounded show improvement on both metrics and settings, while their average variance decreased in the unsupervised setting (cf. standard deviations in parenthesis).

Figure 3 confirms that indeed our loss function is ranked better than the previous one, and, in particular, Figure 3.b shows that, in terms of AP, ours is significantly better across different datasets.

Finally, we also observe that semi-supervised setting almost always performs better than the unsupervised one even having

very few anomalous images (1 up to 7 seven depending on the class), so the effect of using proper anomalies in the training set is a major factor for performance improvement.

**Table 2.** Pixel-wise Average Precision (AP) scores (values in percentage) on the MVTec AD dataset. Cross-category average scores and cross-category average standard deviation (in parenthesis). Under the same supervision (group of two columns), the best performance is in bold.

	semi-supervised		unsupervised	
	baseline	ours	baseline	ours
objects	52.0 (5.8)	<b>53.4 (5.8)</b>	36.6 (4.3)	<b>38.7 (2.3)</b>
textures	50.3 (4.5)	<b>54.7 (4.1)</b>	37.8 (2.8)	<b>40.2 (2.0)</b>
all	51.4 (5.3)	<b>53.8 (5.2)</b>	37.0 (3.8)	<b>39.2 (2.2)</b>

## 7. CONCLUSION

This paper introduced an adaptation for the hypersphere loss functions for anomaly segmentation on images. We have highlighted the drawbacks of the loss function originally used in FCDD [4] (Equation 4) and proposed an alternative loss function (Equation 5).

An evaluation of the statistical significance of the proposition is carried out using pairwise Wilcoxon signed-rank tests, summarized in CD diagrams (Figure 3). Our proposition reaches, on average, better performances (Tables 1 and 2) and is, in general, better ranked regardless of the image category in MVTec-AD.

We highlight that the new loss introduced in this paper can be used with other neural network architectures better designed for segmentation (e.g. U-Net and its improved versions), which we expect to provide further higher improvements.

## 8. REFERENCES

- [1] Lukas Ruff, Jacob R. Kauffmann, Robert A. Vandermeulen, Grégoire Montavon, Wojciech Samek, Marius Kloft, Thomas G. Dietterich, and Klaus-Robert Müller, “A Unifying Review of Deep and Shallow Anomaly Detection,” *Proceedings of the IEEE*, vol. 109, no. 5, pp. 756–795, 2021.
- [2] Guansong Pang, Chunhua Shen, Longbing Cao, and Anton Van Den Hengel, “Deep Learning for Anomaly Detection: A Review,” *ACM Comput. Surv.*, vol. 54, no. 2, Mar. 2021, Place: New York, NY, USA Publisher: Association for Computing Machinery.
- [3] Paul Bergmann, Kilian Batzner, Michael Fauser, David Sattlegger, and Carsten Steger, “The MVTec Anomaly Detection Dataset: A Comprehensive Real-World Dataset for Unsupervised Anomaly Detection,” *International Journal of Computer Vision*, vol. 129, no. 4, pp. 1038–1059, Apr. 2021.
- [4] Philipp Liznerski, Lukas Ruff, Robert A. Vandermeulen, Billy Joe Franks, Marius Kloft, and Klaus Robert Muller, “Explainable Deep One-Class Classification,” in *International Conference on Learning Representations*, 2021.
- [5] Pramuditha Perera, Poojan Oza, and Vishal M. Patel, “One-Class Classification: A Survey,” Tech. Rep. arXiv:2101.03064, arXiv, Jan. 2021, arXiv:2101.03064 [cs] type: article.
- [6] Bernhard Schölkopf, John C. Platt, John Shawe-Taylor, Alex J. Smola, and Robert C. Williamson, “Estimating the Support of a High-Dimensional Distribution,” *Neural Computation*, vol. 13, no. 7, pp. 1443–1471, July 2001.
- [7] David M.J. Tax and Robert P.W. Duin, “Support Vector Data Description,” *Machine Learning*, vol. 54, no. 1, pp. 45–66, Jan. 2004.
- [8] Lukas Ruff, Robert Vandermeulen, Nico Goernitz, Lucas Deecke, Shoaib Ahmed Siddiqui, Alexander Binder, Emmanuel Müller, and Marius Kloft, “Deep One-Class Classification,” in *Proceedings of the 35th International Conference on Machine Learning*, Jennifer Dy and Andreas Krause, Eds. July 2018, vol. 80 of *Proceedings of Machine Learning Research*, pp. 4393–4402, PMLR.
- [9] Lukas Ruff, Robert A. Vandermeulen, Nico Görnitz, Alexander Binder, Emmanuel Müller, Klaus-Robert Müller, and Marius Kloft, “Deep Semi-Supervised Anomaly Detection,” *arXiv:1906.02694 [cs, stat]*, Feb. 2020, arXiv: 1906.02694.
- [10] Lukas Ruff, Robert A. Vandermeulen, Billy Joe Franks, Klaus-Robert Müller, and Marius Kloft, “Re-thinking Assumptions in Deep Anomaly Detection,” *arXiv:2006.00339 [cs, stat]*, July 2021, arXiv: 2006.00339.
- [11] Vitjan Zavrtnik, Matej Kristan, and Danijel Skočaj, “DRAEM - A Discriminatively Trained Reconstruction Embedding for Surface Anomaly Detection,” in *Proceedings of the IEEE/CVF International Conference on Computer Vision (ICCV)*, 2021, pp. 8330–8339.
- [12] Niv Cohen and Yedid Hoshen, “Sub-Image Anomaly Detection with Deep Pyramid Correspondences,” 2020.
- [13] Karsten Roth, Latha Pemula, Joaquin Zepeda, Bernhard Schölkopf, Thomas Brox, and Peter Gehler, “Towards Total Recall in Industrial Anomaly Detection,” in *Proceedings of the IEEE/CVF Conference on Computer Vision and Pattern Recognition (CVPR)*, June 2022, pp. 14318–14328.
- [14] Oliver Rippel, Patrick Mertens, Eike König, and Dorit Merhof, “Gaussian Anomaly Detection by Modeling the Distribution of Normal Data in Pretrained Deep Features,” *IEEE Transactions on Instrumentation and Measurement*, vol. 70, pp. 1–13, 2021, Conference Name: IEEE Transactions on Instrumentation and Measurement.
- [15] Thomas Defard, Aleksandr Setkov, Angélique Loesch, and Romaric Audigier, “PaDiM: A Patch Distribution Modeling Framework for Anomaly Detection and Localization,” in *Pattern Recognition. ICPR International Workshops and Challenges*, Alberto Del Bimbo, Rita Cucchiara, Stan Sclaroff, Giovanni Maria Farinella, Tao Mei, Marco Bertini, Hugo Jair Escalante, and Roberto Vezzani, Eds., Cham, 2021, pp. 475–489, Springer International Publishing.
- [16] JunKyu Jang, Eugene Hwang, and Sung-Hyuk Park, “N-pad : Neighboring Pixel-based Industrial Anomaly Detection,” Oct. 2022, 0 citations (Semantic Scholar/arXiv) [2022-10-25] 0 citations (Semantic Scholar/DOI) [2022-10-25] arXiv:2210.08768 [cs].
- [17] Jaehyeok Bae, Jae-Han Lee, and Seyun Kim, “Image Anomaly Detection and Localization with Position and Neighborhood Information,” Nov. 2022, 0 citations (Semantic Scholar/arXiv) [2022-11-28] arXiv:2211.12634 [cs].
- [18] Yeongmin Kim, Huiwon Jang, DongKeon Lee, and Ho-Jin Choi, “AltUB: Alternating Training Method to Update Base Distribution of Normalizing Flow for Anomaly Detection,” Oct. 2022, 0 citations (Semantic Scholar/arXiv) [2022-11-01] arXiv:2210.14913 [cs] version: 1.